Acta Astronautica 165 (2019) 158–166

Contents lists available at ScienceDirect

Acta Astronautica

journal homepage: www.elsevier.com/locate/actaastro

Luni-solar resonances and effect on long-term evolution of inclined geostationary transfer orbits

Xuhui Luo, Yue Wang*

School of Astronautics, Beihang University, No.9 South Third Street, Shahe Higher Education Park, Changping District, Beijing 102206, China

ARTICLE INFO

Keywords:
Inclined geostationary transfer orbits
Semi-analytical dynamic model
Luni-solar secular resonances
Long-term dynamical evolution

ABSTRACT

In this paper, a singly-averaged, semi-analytical orbital dynamic model in terms of Milankovitch elements is given for geostationary transfer orbits (GTOs), which includes the Earth's oblateness, luni-solar perturbations, atmospheric drag and solar radiation pressure (SRP). The orbital dynamic model is verified through a numerical simulation compared with the Semi-analytic Tool for End of Life Analysis software (STELA) by CNES. We find that if the area-to-mass ratio of the object is relatively large, the SRP will have a significant impact on the long-term evolution of GTOs. Then, the long-term dynamical evolution and orbital resonances of rocket upper stages in inclined geostationary transfer orbits (IGTOs) are studied. It has been found that the luni-solar secular resonances, which are inclination-dependent-only, play a leading role in the long-term evolution of IGTOs. By comparing and analyzing long-term dynamical evolution of orbits with different initial inclinations, the effects of luni-solar secular resonances are studied in details. Finally, a mitigation method for IGTO objects by utilizing luni-solar secular resonances is proposed, in which the eccentricity growth caused by the resonances is used for an early atmospheric re-entry.

1. Introduction

With the increase of space activities, a large amount of space debris of various sizes has been created in Earth orbits and the number is still increasing rapidly. The growing number of space debris makes the collision risk between one of them and an operational spacecraft remarkable, posing a great threat to the operational spacecraft. For this reason, the Inter-Agency Space Debris Coordination Committee (IADC) has defined two orbital protection regions: region A for low Earth orbits (LEOs) (altitude $<$ 2000 km) and region B for geostationary orbits (GEOs) (GEO – 200 km $<$ altitude $<$ GEO + 200 km; inclination $<$ 15 deg or $>$ 165 deg) [1].

Nowadays, space debris mitigation has become a global concern for both space agencies and private contractors. The passive means of space debris mitigation, which utilize the natural perturbations and the resulting dynamical evolution and resonances, are particularly attractive in terms of low cost and simpleness. As a result, the long-term dynamical evolution, luni-solar resonances, and possible passive means of space debris mitigation of all types of Earth orbits have been investigated extensively and have been a spotlight of the community for recent years [2–4].

The geostationary transfer orbits (GTOs) are a special type of Earth orbits, and are highly related to the space debris mitigation. GTOs are characterized by a low perigee (160 km–1000 km) and a high apogee (altitude typically identical to that of geostationary satellites), and, then, will cross both the LEO and GEO orbital protection regions. Therefore, the upper stages of launch vehicles left on GTOs during launching GEO satellites will pose serious threats to the operational spacecraft in both the orbital protection regions. Because of its low perigee and high apogee, the objects on GTOs are subjected to multiple perturbations and their interactions, including the Earth's oblateness, atmospheric drag, luni-solar perturbations and solar radiation pressure (SRP). A thorough understanding of dynamical behaviors is fundamental to the mitigation of space debris in GTOs.

Many researchers have studied the dynamical evolution, decay, and lifetime of GTOs, and they all have found that initial launch time or conditions have a strong impact on the orbital lifetime under luni-solar perturbations and their interaction with atmospheric drag [5–8]. Recently, Wang and Gurfil [9,10] have established a semi-analytical orbital dynamics model in terms of Milankovitch elements to analyze the orbital lifetime of GTOs as well as the important role of the solar apsidal resonance. Skoulidou et al. [11] applied a more visual 2-D lifetime maps, which recorded the dynamical lifetime for GTOs, to study this problem.

However, there are few studies focused on the dynamical evolution of inclined geostationary transfer orbits (IGTOs), where the upper

* Corresponding author.
E-mail addresses: xhluo@buaa.edu.cn (X. Luo), ywang@buaa.edu.cn (Y. Wang).

https://doi.org/10.1016/j.actaastro.2019.09.005
Received 9 December 2018; Received in revised form 2 July 2019; Accepted 5 September 2019
Available online 09 September 2019

stages of launch vehicles were left during launching inclined geosynchronous orbit (IGSO) satellites of the Chinese Beidou satellite navigation system. Due to its large inclination (about 55°), the dynamical behaviors of the IGTOs are distinct from those of the low-inclination GTOs. The low-inclination GTOs have an important feature during their evolution, the solar apsidal resonance, i.e., the 1:1 resonance between the solar apparent orbital motion and the rotation of the orbital apsidal line caused by Earth's oblateness [10]. However, due to the large inclination, the solar apsidal resonance will not occur during evolution of IGTOs. Particularly, since IGTO's inclination is just located in the region of luni-solar secular resonances, which are inclination-dependent-only, its evolution is mainly affected by the luni-solar secular resonances. The luni-solar secular resonances will make the orbit eccentricity increase or decrease significantly, which in turn prominently affects the evolution of the perigee height and the orbital lifetime.

The extended study of luni-solar secular resonances starts at the research on the large eccentricity growth of operational and disposal orbits of the global navigation satellite systems (GNSS) in the medium Earth orbits (MEOs) region. Under the luni-solar perturbations and the Earth's oblateness, there is a large eccentricity growth of the navigation satellite orbits due to the luni-solar secular resonance [12]. Rossi [13] used numerical integrations to investigate the stability of the orbits of the navigation constellations and Deleflie et al. [16] also found that the initial conditions have a large impact on the eccentricity growth. Because of the instability of disposal orbits caused by luni-solar secular resonances, Anselmo and Pardini [14,15] specially investigated dynamical evolution and environmental impact in MEOs of all the abandoned spacecraft and upper stages associated and found that the upper stage disposal strategies used so far for Beidou and Galileo have generally been quite successful. Alessi et al. [17] studied the complex dynamics of the MEO region and defined a map of the resonances with the aim of finding the best disposal orbits. Bordovitsyna et al. [18,19] studied the resonances from another perspective and found that secular resonances affecting these objects may give rise to dynamic randomness in their long-term evolution. Kuznetsov and Avvakumova [20] also found that due to the luni-solar secular resonances space debris in the vicinity of GNSS regions can pass through the regions of operational spacecraft.

However, currently there is little research on the luni-solar secular resonances and their impacts on the orbital evolution for IGTOs with a large eccentricity, which will have different behaviors with MEOs studied before. In this paper, we will investigate luni-solar secular resonances and the associated problems of orbital evolution and lifetime reduction of IGTOs. This research will be carried out based on a simple, but effective, averaged orbital dynamics model formulated in terms of Milankovitch elements.

The main contributions of this paper are as follows: Through averaging the SRP, a more precise semi-analytical averaged orbital dynamics model of IGTOs will be established based on the singly-averaged dynamical model in previous work [9], which accounted for the main effects of the Earth oblateness, luni-solar perturbations, and atmospheric drag. The averaged dynamical model will be verified through a numerical simulation compared with the Semi-analytic Tool for End of Life Analysis software (STELA) by CNES. Then, we will study the long-term dynamical evolution and luni-solar secular resonances of IGTOs and explain the underlying dynamical mechanism of the luni-solar secular resonances based on the doubly-averaged variational equation of the eccentricity. By comparing and analyzing long-term dynamical evolution of orbits with different initial inclinations, the effects of luni-solar secular resonances are investigated in details. Finally, a mitigation method for IGTO objects by utilizing luni-solar secular resonances is proposed, in which the eccentricity growth caused by the resonances is used for an early atmospheric re-entry.

2. Dynamical model

The concept of averaging is used to evaluate the secular effects of the perturbations and the singly-averaged equations are derived by averaging the equations of variation over the orbit period thus eliminating all short orbit period terms. The resulting variational equations are significantly simpler and the dominant long-term and secular variations due to a particular force can be identified [12].

In the averaged orbital dynamic model, we adopted the Milankovitch elements to describe orbits. The orbital equations formulated in terms of Milankovitch elements are suitable for the orbital dynamical analysis due to their concise vectorial form and explicit relation with the underlying physics. The Milankovitch elements contain two vectorial integrals: the specific angular momentum vector $\boldsymbol{H}$, normal to the instantaneous orbital plane, and the Laplace vector $\boldsymbol{b} = \mu \boldsymbol{e}$, pointing towards the instantaneous perigee, where μ is the gravitational constant of the Earth and $\boldsymbol{e}$ is the eccentricity vector [21]. The vectors $\boldsymbol{H}$ and $\boldsymbol{e}$ can be written in terms of the position $\boldsymbol{r}$ and velocity $\boldsymbol{v}$ as

$$\boldsymbol{H}=\boldsymbol{r}^{\times}\boldsymbol{v}, \tag{1}$$

$$\boldsymbol{e} = \frac{1}{\mu}\boldsymbol{v}^{\times}\boldsymbol{r}^{\times}\boldsymbol{v} - \frac{\boldsymbol{r}}{r}, \tag{2}$$

where the notation $\boldsymbol{r}^{\times}$ denotes the cross-product dyadic, i.e., $\boldsymbol{r}^{\times}\boldsymbol{v} = \boldsymbol{r} \times \boldsymbol{v}$ and $\boldsymbol{v}^{\times}\boldsymbol{r}^{\times}\boldsymbol{v} = \boldsymbol{v} \times (\boldsymbol{r} \times \boldsymbol{v})$.

In a previous paper [9], the singly-averaged orbital dynamics for $\boldsymbol{H}$ and $\boldsymbol{e}$ subjected to the perturbations of J_2, luni-solar third-body gravity, and atmospheric drag are given by

$$\begin{aligned}\dot{\mathrm{H}} &= \dot{\mathrm{H}}_{J_2} + \dot{\mathrm{H}}_S + \dot{\mathrm{H}}_M + \dot{\mathrm{H}}_{Atm}\\ &= -\frac{3\mu J_2 R_E^2}{2a^3h^5}(\hat{\mathrm{p}}\cdot\mathrm{h})\hat{\mathrm{p}}^{\times}\mathrm{h}\\ &\quad+\frac{3a^2\mu_S}{2d_S^3}[5(\hat{\mathrm{d}}_S\cdot\mathrm{e})\mathrm{e}^{\times}\hat{\mathrm{d}}_S-(\hat{\mathrm{d}}_S\cdot\mathrm{h})\mathrm{h}^{\times}\hat{\mathrm{d}}_S]\\ &\quad+\frac{3a^2\mu_M}{2d_M^3}[5(\hat{\mathrm{d}}_M\cdot\mathrm{e})\mathrm{e}^{\times}\hat{\mathrm{d}}_M-(\hat{\mathrm{d}}_M\cdot\mathrm{h})\mathrm{h}^{\times}\hat{\mathrm{d}}_M]\\ &\quad-\frac{1}{2}B\sqrt{\frac{\mu(1-e^2)}{2a\pi z}}\rho_{p_0}\exp\left(\frac{r_{p0}-r_p}{H_\rho}\right)(1+K_1)\mathrm{H},\end{aligned} \tag{3}$$

$$\begin{aligned}\dot{\mathrm{e}} &= \dot{\mathrm{e}}_{J_2} + \dot{\mathrm{e}}_S + \dot{\mathrm{e}}_M + \dot{\mathrm{e}}_{Atm}\\ &= -\frac{3nJ_2R_E^2}{4a^2h^5}\left\{\left[1-\frac{5}{h^2}(\hat{\mathrm{p}}\cdot\mathrm{h})^2\right]\mathrm{h}^{\times}+2(\hat{\mathrm{p}}\cdot\mathrm{h})\hat{\mathrm{p}}^{\times}\right\}\mathrm{e}\\ &\quad+\frac{3\mu_S}{2nd_S^3}[5(\hat{\mathrm{d}}_S\cdot\mathrm{e})\mathrm{h}^{\times}\hat{\mathrm{d}}_S-(\hat{\mathrm{d}}_S\cdot\mathrm{h})\mathrm{e}^{\times}\hat{\mathrm{d}}_S-2\mathrm{h}^{\times}\mathrm{e}]\\ &\quad+\frac{3\mu_M}{2nd_M^3}[5(\hat{\mathrm{d}}_M\cdot\mathrm{e})\mathrm{h}^{\times}\hat{\mathrm{d}}_M-(\hat{\mathrm{d}}_M\cdot\mathrm{h})\mathrm{e}^{\times}\hat{\mathrm{d}}_M-2\mathrm{h}^{\times}\mathrm{e}]\\ &\quad-B\frac{1+e}{a\sqrt{2\pi z}}\rho_{p_0}\exp\left(\frac{r_{p0}-r_p}{H_\rho}\right)(1+K_2)H\hat{\mathrm{e}},\end{aligned} \tag{4}$$

where $(\hat{\cdot})$ denotes the unit vector, R_E is the mean equatorial radius of the Earth, $\mathbf{h} = \mathbf{H}/\sqrt{\mu a}$ is the scaled orbital angular momentum, a is the semi-major axis, $n = \sqrt{\mu/a^3}$ is the mean motion of the GTO, $\hat{\mathrm{p}}$ is the spin axis of Earth, μ_S and μ_M are the gravitational constants of the Sun and Moon, respectively, $\mathbf{d}_S$ and $\mathbf{d}_M$ denote the position vectors of the Sun and Moon relative to Earth, respectively, $B = SC_D/m$ is the ballistic coefficient of the GTO object, S/m is the area-to-mass ratio (AMR), C_D is the non-dimensional drag coefficient with a typical value of 2.2, $r_p = a(1-e)$, $z = ae/H_\rho$, H_ρ is the constant scale height in the exponential atmospheric density model, $\rho = \rho_{p_0}\exp[-(r-r_{p_0})/H_p]$, ρ_{p_0} and r_{p_0} are the atmospheric density and distance from the Earth center at initial perigee, respectively, and

$$K_1 = \frac{1+3e^2}{8z(1-e^2)}, \quad K_2 = \frac{3e^2-4e-3}{8z(1-e^2)}. \tag{5}$$

However, the singly-averaged semi-analytical orbital dynamic model (3)–(4) does not take into account the SRP. If the AMR is relatively large, the SRP will have a significant impact on the long-term

evolution of GTOs. Additionally, although in low Earth orbits, quite a number of resonances associated with SRP are detected and play a significant role in the dynamical evolution [27]. Therefore, we need to add the SRP to the averaged dynamic model to make it applicable to more cases.

In averaged dynamic models, since we only need to evaluate the secular effects of the perturbations, we apply the cannonball model to deal with the SRP acceleration, which treats the object as a sphere with constant optical properties. Any force component normal to the object-Sun line that results from an aspherical shape or non-uniformly reflecting surface is thereby neglected. Then, the net acceleration will act in the direction directly away from this line and have the general form

$$\mathbf{a}_{srp} = -(1+\alpha)(S/m)P_{\Phi}\frac{(\mathbf{d}_S - \mathbf{r})}{|\mathbf{d}_S - \mathbf{r}|^3} = -\beta\frac{(\mathbf{d}_S - \mathbf{r})}{|\mathbf{d}_S - \mathbf{r}|^3}, \tag{6}$$

where α is the reflectance of the object, S/m is the appropriate cross-sectional area-to-mass ratio in m^2/kg, P_{Φ} is the solar radiation constant approximately equal to $1 \times 10^8 kg{\cdot}km^2/(s^2{\cdot}m^2)$, and $\beta = (1+\alpha)(S/m)P_{\Phi}$ [22].

According to previous results [22], the averaged SRP dynamics is given by

$$\dot{\mathbf{h}}_{srp} = -\frac{3}{2}\sqrt{\frac{a}{\mu}}\frac{\beta}{d_S^2}\hat{\mathbf{d}}_S^{\times}\mathbf{e}, \tag{7}$$

$$\dot{\mathbf{e}}_{srp} = -\frac{3}{2}\sqrt{\frac{a}{\mu}}\frac{\beta}{d_S^2}\hat{\mathbf{d}}_S^{\times}\mathbf{h}. \tag{8}$$

Multiplying Eq. (7) both sides by $\sqrt{\mu a}$, one gets

$$\dot{\mathbf{H}}_{srp} = -\frac{3}{2}\frac{a\beta}{d_S^2}\hat{\mathbf{d}}_S^{\times}\mathbf{e}. \tag{9}$$

Thus, we have got the averaged variational equations under the effects of the SRP. Substituting Eqs. (8) and (9) into Eqs. (3) and (4), the resultant singly-averaged, semi-analytical orbital dynamics of $\boldsymbol{H}$ and $\boldsymbol{e}$ under J_2, luni-solar perturbations, atmospheric drag, and SRP are given by

$$\begin{aligned}\dot{\mathrm{H}} &= \dot{\mathrm{H}}_{J_2} + \dot{\mathrm{H}}_S + \dot{\mathrm{H}}_M + \dot{\mathrm{H}}_{Atm} + \dot{\mathrm{H}}_{srp}\\ &= -\tfrac{3\mu J_2 R_E^2}{2a^3h^5}(\hat{\mathrm{p}}\cdot\mathrm{h})\hat{\mathrm{p}}^{\times}\mathrm{h}\\ &+ \tfrac{3a^2\mu_S}{2d_S^3}[5(\hat{\mathrm{d}}_S\cdot\mathrm{e})\mathrm{e}^{\times}\hat{\mathrm{d}}_S - (\hat{\mathrm{d}}_S\cdot\mathrm{h})\mathrm{h}^{\times}\hat{\mathrm{d}}_S]\\ &+ \tfrac{3a^2\mu_M}{2d_M^3}[5(\hat{\mathrm{d}}_M\cdot\mathrm{e})\mathrm{e}^{\times}\hat{\mathrm{d}}_M - (\hat{\mathrm{d}}_M\cdot\mathrm{h})\mathrm{h}^{\times}\hat{\mathrm{d}}_M]\\ &- \tfrac{1}{2}B\sqrt{\tfrac{\mu(1-e^2)}{2a\pi z}}\rho_{p_0}\exp\left(\tfrac{r_{p0}-r_p}{H_\rho}\right)(1+K_1)\mathrm{H}\\ &- \tfrac{3}{2}\tfrac{a\beta}{d_S^2}\hat{\mathrm{d}}_S^{\times}\mathrm{e},\end{aligned} \tag{10}$$

$$\begin{aligned}\dot{\mathrm{e}} &= \dot{\mathrm{e}}_{J_2} + \dot{\mathrm{e}}_S + \dot{\mathrm{e}}_M + \dot{\mathrm{e}}_{Atm} + \dot{\mathrm{e}}_{srp}\\ &= -\tfrac{3nJ_2R_E^2}{4a^2h^5}\left\{\left[1 - \tfrac{5}{h^2}(\hat{\mathrm{p}}\cdot\mathrm{h})^2\right]\mathrm{h}^{\times} + 2(\hat{\mathrm{p}}\cdot\mathrm{h})\hat{\mathrm{p}}^{\times}\right\}\mathrm{e}\\ &+ \tfrac{3\mu_S}{2nd_S^3}[5(\hat{\mathrm{d}}_S\cdot\mathrm{e})\mathrm{h}^{\times}\hat{\mathrm{d}}_S - (\hat{\mathrm{d}}_S\cdot\mathrm{h})\mathrm{e}^{\times}\hat{\mathrm{d}}_S - 2\mathrm{h}^{\times}\mathrm{e}]\\ &+ \tfrac{3\mu_M}{2nd_M^3}[5(\hat{\mathrm{d}}_M\cdot\mathrm{e})\mathrm{h}^{\times}\hat{\mathrm{d}}_M - (\hat{\mathrm{d}}_M\cdot\mathrm{h})\mathrm{e}^{\times}\hat{\mathrm{d}}_M - 2\mathrm{h}^{\times}\mathrm{e}]\\ &- B\tfrac{1+e}{a\sqrt{2\pi z}}\rho_{p_0}\exp\left(\tfrac{r_{p0}-r_p}{H_\rho}\right)(1+K_2)H\hat{\mathrm{e}}\\ &- \tfrac{3}{2}\sqrt{\tfrac{a}{\mu}}\tfrac{\beta}{d_S^2}\hat{\mathrm{d}}_S^{\times}\mathrm{h}.\end{aligned} \tag{11}$$

3. Orbital dynamics model verification

To verify the averaged orbital model (10)–(11), a numerical simulation is carried out and compared with STELA by CNES (The French Space Agency).

3.1. Initial conditions and system parameters setting

The epoch time is set to be 21 March 2018 00:00:00 UTC, and the orbits will be propagated for 10 years. The initial orbital elements of the GTO are defined as

$$h_{a0} = 35809\text{km},\ i_0 = 6°,\ h_{p0} = 350\text{km},\ \omega_0 = 178°, \tag{12}$$

where h_{a0} and h_{p0} are the initial values of the apogee height and perigee height, respectively. The initial RAAN and mean anomaly are chosen as

$$\Omega_0 = 177°, \quad M_0 = 0° \tag{13}$$

To be more conservative in the model verification, we chose a relatively high AMR, which implies more significant effects of SRP and atmospheric drag,

$$S/m = 0.1, \quad C_D = 2.2, \quad C_r = 1.5. \tag{14}$$

3.2. Simulation results and discussion

The orbital elements of interest are the semi-major axis a, the eccentricity e, and the perigee height $h_p = a(1-e) - R_E$. Time histories of a, e, and h_p propagated by our orbital model with SRP, previous orbital model without SRP, and STELA are given in Figs. 1–3, respectively.

As shown by Figs. 1–3, the new model with SRP agrees better with STELA than the previous model without SRP within the first ten years, which means that adding the effects of SRP makes the model more precise. Particularly, the influence of SRP on the long-term evolution of GTOs cannot be neglected in such initial conditions (AMR is larger than 0.1).

At the same time, it is found that under the effects of SRP, the GTO shows some different characteristics during the long-term evolution. Although the semi-major axis and eccentricity all have short-period oscillations, the SRP makes semi-major axis and eccentricity decay more slowly, as shown by Figs. 1–2. As stated before, in the dynamical model (10-11), the effects of the Earth's shadow are not taken into account, so the SRP can be regarded as a conservative force. Theoretically, the conservative force cannot have any impact on the semi-major axis in the long-term evolution. However, from Figs. 2–3, it can be seen that the SRP enhances the oscillation of eccentricity and cause both the oscillation amplitude and mean value of perigee height much larger. This phenomenon has also been found in the evolution of high-Earth orbits [22,23]. Then, the increase of the perigee height leads to a minor effect of the atmospheric drag on the evolution, which in the end makes the semi-major axis decay more slowly.

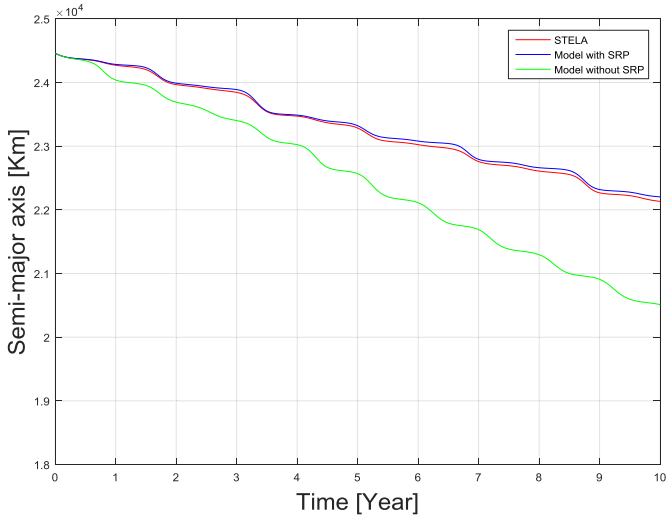

Fig. 1. Time history of the semi-major axis a.

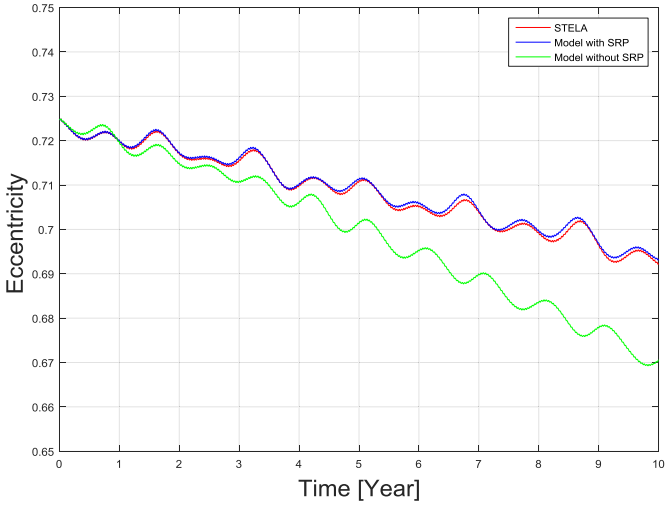

Fig. 2. Time history of the eccentricity e.

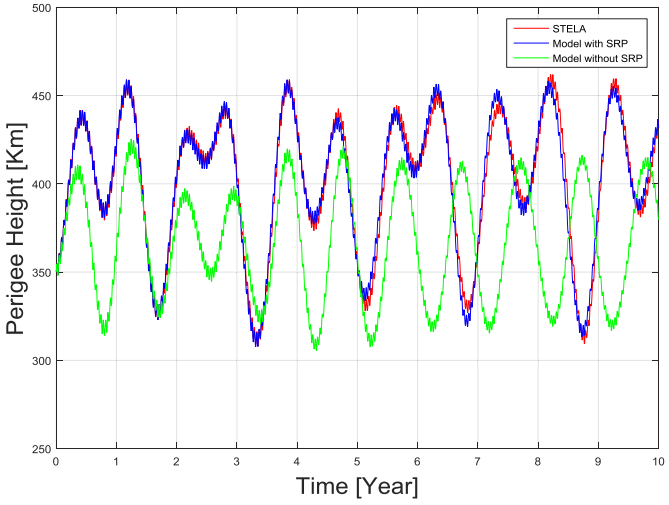

Fig. 3. Time history of the perigee height h_p.

In conclusion, after taking into account the SRP, the model becomes more precise, and it can capture better the important features of the long-term evolution of GTOs.

4. Luni-solar resonances

Due to the periodic orbital motion of the Sun and Moon, their perturbing effects on a satellite's orbit are also periodic. Obviously, we can reflect the periodicity in the expansion of their disturbing potentials as functions of the satellite's orbital elements. In such expansions (see Eqs. 3–11 in Ref. [24]) cosine terms occur having arguments of the form $\delta\psi$, where

$$\psi = \lambda\omega + \eta\Omega + \kappa M + U, \tag{15}$$

δ, λ, η and κ are integers, and U is a linear function of ω_{3B} , the argument of perigee, M_{3B}, the mean anomaly, and Ω_{3B}, the longitude of the ascending node of either the Moon's or the Sun's orbit with respect to the Earth's equator. Under certain circumstances, the argument $\delta\psi$ associated with these resonant terms will be approximately a constant, i.e.,

$$\dot{\psi} = \lambda\dot{\omega} + \eta\dot{\Omega} + \kappa\dot{M} + \dot{U} \approx 0. \tag{16}$$

Luni-solar resonances occur for orbits that satisfy the commensurability condition (16). In such cases, some orbital elements, such as the eccentricity, will suffer a quasi-secular variation as a result of large period of the oscillation in the resonance term [24].

Clearly, luni-solar resonances can be classified into different types according to the commensurability condition, i.e., the values of δ, λ, η, κ, and the coefficients of U [24]. Here, we only consider a class of luni-solar resonances, which are inclination-dependent-only and have remarkable effect on the long-term evolution of the eccentricity. The inclination of IGTOs is just located in the region of such resonances, which satisfy the commensurability

$$\dot{\psi} = \lambda\dot{\omega} + \eta\dot{\Omega} \approx 0. \tag{17}$$

The doubly-averaged variational equation of $\boldsymbol{e}$ can be derived by further removing 6-month and 14-day short-period terms caused by the apparent orbital motions of the Sun and Moon from the singly-averaged equations [25]. According to Refs. [12,25], a closed form of the doubly-averaged variational equation of $\boldsymbol{e}$ due to third-body perturbations is derived via a computerized series expansion and is given as:

$$\begin{aligned}\dot{e} = &-\frac{15}{16}e\gamma s[C_1 \sin 2(\omega - \Delta\Omega) + C_2 \sin(2\omega - \Delta\Omega)\\ &+ C_3 \sin 2\,\omega + C_4 \sin(2\omega + \Delta\Omega) + C_5 \sin 2(\omega + \Delta\Omega)],\end{aligned} \tag{18}$$

where $\gamma = n_{3B}^2 R_m/n$, $s = (1 - e^2)^{1/2}$, n is the mean motion of the orbit, n_{3B} is the mean motion of the third body, R_m is the mass ratio (=1 for solar perturbation, = 1/81.3 for lunar perturbation) and $\Delta\Omega = \Omega - \Omega_{3B}$.

The five coefficients in Eq. (18) are functions of the inclination with the following form,

$$\begin{aligned}C_1 &= \sin^2 i_{3B}(\cos i + 1/2 \sin^2 i - 1),\\ C_2 &= \sin i \sin 2i_{3B}(\cos i - 1),\\ C_3 &= 2 \sin^2 i(3/2 \sin^2 i_{3B} - 1),\\ C_4 &= \sin i \sin 2i_{3B}(\cos i + 1),\\ C_5 &= \sin^2 i_{3B}(1/2 \sin^2 i - \cos i - 1),\end{aligned} \tag{19}$$

where i_{3B} is the inclination of the third body.

It can be easily found that the periodic oscillation of e in Eq. (18) is induced by the periodic motions of the RAAN, Ω, and the argument of perigee, ω, which are mainly caused by the Earth's oblateness. The time rates of Ω and ω caused by J_2 are

$$\dot{\Omega}_{J_2} = -1.5 J_2 \sqrt{\mu} R_E^2 \frac{\cos i}{a^{7/2}(1 - e^2)^2}, \tag{20}$$

$$\dot{\omega}_{J_2} = 0.75 J_2 \sqrt{\mu} R_E^2 \frac{5\cos^2 i - 1}{a^{7/2}(1 - e^2)^2}. \tag{21}$$

Therefore, the ratio of time rates of Ω and ω mainly depends on the inclination of the orbit

$$\frac{\omega - \omega_0}{\Omega - \Omega_0} \approx \frac{\dot{\omega}_{J_2}}{\dot{\Omega}_{J_2}} = -\frac{5\cos^2 i - 1}{2\cos i}. \tag{22}$$

From Eq. (22), when the orbits satisfy the commensurability condition (17) depending only on the inclinations, then the luni-solar secular resonances are called the inclination-dependent-only resonances. More specifically, if one of the sine terms in Eq. (18), listed in Table 1, satisfies the commensurability condition (17), the orbital eccentricity will suffer a quasi-secular variation, resulting in a much longer period of the eccentricity e. The phenomenon will have a significant impact on the orbital evolution and orbital lifetime.

As stated above, the initial orbital inclination of the rocket upper stages on IGTOs generated by the Beidou navigation is about 55°. At this inclination, the time rate of 2ω nearly cancels the rate of Ω, resulting in the luni-solar secular resonances. The evolutionary analysis of the IGTO with luni-solar secular resonances is of great significance for us to reduce space debris in this orbital region.

We propagated a standard IGTO launched by CZ-3[1] numerically as in Eq. (23) by using the dynamical model (10)–(11) to show the luni-solar secular resonance and analyze its effect on the orbital evolution,

Table 1
The time rates of certain terms in Eq. (18) with different inclinations.

Inclination	Term
46.38°	$\dot{\omega} + \dot{\Omega} \approx 0$
56.06°	$2\dot{\omega} + \dot{\Omega} \approx 0$
63.44°	$\dot{\omega} \approx 0$
69.01°	$2\dot{\omega} - \dot{\Omega} \approx 0$
73.15°	$\dot{\omega} - \dot{\Omega} \approx 0$

taking the following data:

$$h_{a0} = 35809\text{km},\ i_0 = 55°, h_{p0} = 250\text{km},\quad \omega_0 = 178°. \tag{23}$$

Fig. 4 and Fig. 5 show the perigee height h_p evolutionary histories and orbital lifetime distribution with different initial RAAN, ranging from 0° to 360°, which corresponds to different launch hours during one day. The epochs are chosen as the Spring Equinox and Summer Solstice in 2018, respectively. The AMR of the IGTO object is set to be $S/m = 0.008\ \text{m}^2/\text{kg}$. The time step of the simulations is 86400 s. When the perigee height of the IGTO is lower than 100 km, the IGTO will be regarded to have been decayed, causing the simulation end.

By comparing Figs. 4 and 5, it can be easily found that the epoch time had little impact on the dynamical evolution of the h_p and the orbital lifetime distribution. Generally, the epoch time determines the initial orientation of the Sun and Moon relative to the Earth, indicating that the luni-solar secular resonances are not sensitive to the initial orientation of the Sun and Moon. This conclusion was expected, since the luni-solar secular resonance reflects the secular effects of the luni-solar third-body gravity, in which the short-period effects associated with the apparent orbital motions of the Sun and Moon have been averaged out.

From Figs. 4–5, it can also be seen that there is a relatively long oscillation period of the perigee height in certain initial conditions due to the luni-solar secular resonances, and especially, the orbital lifetime is highly dependent on Ω_0. Generally, the initial argument of perigee ω_0 of GTOs is about 180°, and, therefore, the most important factor affecting the orbital lifetime will be the initial RAAN.

Notice that the orbital lifetime is highly dependent on the evolution of perigee height and only the magnitude of e affects the perigee height. According to the results of Wang and Gurfil [9], we can get a simplified form of the long-period change rate of e caused by the luni-solar perturbations

$$\dot{e} = -\sum_{3B=S,M} \frac{15\mu_{3B}}{4na_{3B}^3 h_{3B}^3}(\hat{\mathrm{H}}_{3B}\cdot\mathrm{e})(\mathrm{h}^{\times}\hat{\mathrm{H}}_{3B})\cdot\hat{\mathrm{e}}, \tag{24}$$

where $h_{3B} = \sqrt{1-e_{3B}^2}$; a_{3B}, e_{3B} and H_{3B} are the semi-major axis, eccentricity, and angular momentum of the orbit of the Sun or Moon, respectively. Eq. (24) is identical with Eq. (18) essentially, but Eq. (24) has a more concise vector form. Fig. 6 shows the long-period eccentricity change per day with $i = 55°$ calculated by Eq. (24) and we can use this figure to explain the orbital lifetime distribution in Figs. 4 and 5. Fig. 6 also seems to be a pendulum structure, which is somewhat similar to the resonances in LEO studied by Celletti and Gales [26]. Although the structure is similar, this type of resonances cannot be analyzed analytically as in the Ref. [26] due to the semi-analytical form of Eq. (24).

Furthermore, Figs. 6 and 4 show that, in the interval $10° \le \Omega_0 \le 170°$ (the black line) with an initial decrease phase, the eccentricity will decrease at first, in the end resulting in a relatively longer orbital lifetime. On the contrary, in the interval $\Omega_0 > 170°$ (the red line) with an initial increase phase, the eccentricity will increase initially, in the end resulting in a short orbital lifetime. In other words, different values of Ω_0 will lead to different initial value of terms in Eq. (18), result in different initial phases of the long-period oscillations of the eccentricity, and then will lead to distinct long-term dynamical evolution of the perigee height and distinct orbital lifetime.

Particularly, we choose a specific initial condition for the longer orbital lifetime to analyze the effects of the luni-solar secular resonances on the dynamical evolution of IGTOs. The initial conditions are set to be $\Omega_0 = 70°$ with other orbital elements given by Eq. (23), identical with the former case. Time histories of e, h_p, and orbital trajectory evolution on the $\Omega - \omega$ plane are given in Figs. 7–9, respectively.

For comparison, we choose another specific initial condition for the shorter orbital lifetime. The initial RAAN is set to be $\Omega_0 = 200°$, and other orbital elements are identical with the former case. Time histories of e, h_p, and orbital trajectory evolution on the $\Omega - \omega$ plane are given in Figs. 10–12, respectively.

From Figs. 10–12, we can see that on the contrast, if the initial orbital elements have an increase initial phase for the long-period oscillation of the eccentricity, the perigee height will be lowered significantly at first as a result of the long-period oscillation, and the upper stages on the IGTO will re-enter the atmosphere directly, almost giving no threats to the operational spacecraft.

For these reasons, the luni-solar secular resonances can be used to achieve the purpose of space debris mitigation. By adjusting the launch timing of the IGSO satellites of the Beidou satellite navigation system, it is possible to select the appropriate initial RAAN for the IGTO. Under the effects of the luni-solar secular resonances, the orbital eccentricity will increase at first, and the perigee height will be lowered by luni-solar perturbations to the atmosphere directly and rapidly as in the cases of $\Omega_0 > 170°$ in Figs. 4–6.

5. Analysis of luni-solar resonances with different inclinations

In order to further study the luni-solar resonances, we propagated certain standard IGTOs with different orbital inclinations. In this regard, the evolution of eccentricity e and comparative analysis of luni-solar secular resonances are studied.

Fig. 13 shows the time histories of the eccentricity with different inclinations, and most of the inclinations are located at the resonance regions in Table 1. As shown in Fig. 13, the evolution of eccentricity presents different characteristics, especially the distinct periods. For example, with the inclination of 56.06°, where the time rate of the angle $(2\omega + \Omega)$ is close to zero, the luni-solar secular resonances play an important role in the evolution of the eccentricity, resulting in a very-long-period oscillation of the eccentricity. According to the analysis in Section 4, the orbital evolution will experience a complete, long period with an orbital lifetime about 150 years. Theoretically, if the orbital inclination keeps at 56.06°, the period of the long-period oscillation will become infinitely long. However, since the luni-solar perturbations will change the inclination periodically within a small interval, the resonance term $(2\omega + \Omega)$ will change slowly, causing the long period shortened. If we reduce the initial orbital inclination to slightly deviate from the resonance zone, for example setting the inclination equal to 55°, the long period of the evolution of e will be reduced to about 20 years further, as shown by Fig. 7. When the orbital inclination is reduced to 50°, since the inclination is fairly far from the resonance region, it can be basically regarded as that no luni-solar secular resonances occur.

From Fig. 13, it can also be found that the orbit does not undergo luni-solar secular resonances during the evolution, although the orbital inclination is in the resonance region of 46.38°. To find out the reason, we calculate the five coefficients for the inclination of 46.38° in Eq. (19),

[1] The orbital elements are derived from http://www.satlist.nl/.

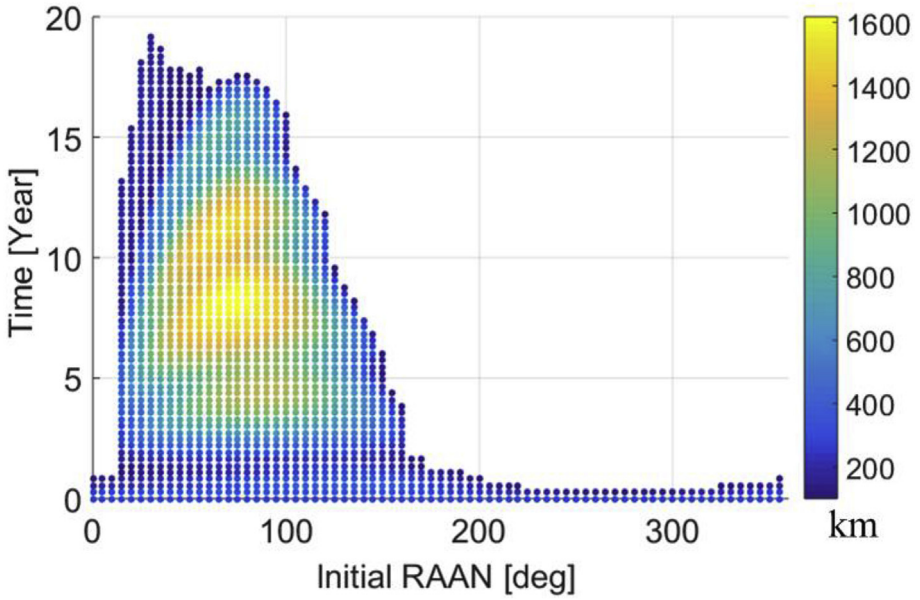

Fig. 4. The perigee height evolutionary histories and orbital lifetime distribution with different Ω_0 (Spring Equinox), and the color bar denotes the perigee height. (For interpretation of the references to color in this figure legend, the reader is referred to the Web version of this article.)

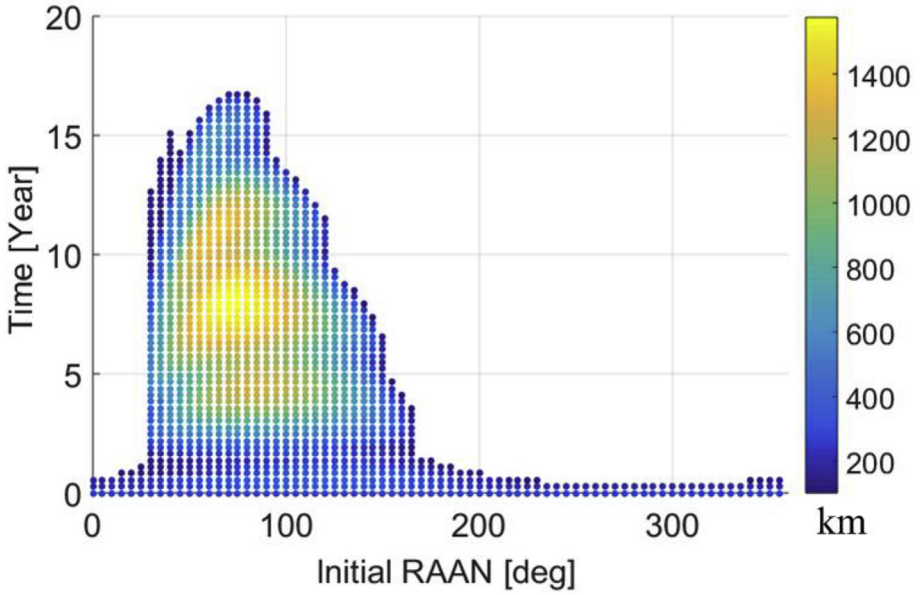

Fig. 5. The perigee height evolutionary histories and orbital lifetime distribution with different Ω_0 (Summer Solstice), and the color bar denotes the perigee height. (For interpretation of the references to color in this figure legend, the reader is referred to the Web version of this article.)

$$C_1 = -0.0076, \quad C_2 = -0.1642, \quad C_3 = -0.7982, \quad C_4 = 0.8947, \quad C_5 = -0.2270. \tag{25}$$

The coefficient C_5 of the resonance term $(\omega + \Omega)$ in the case of 46.38° is much smaller than the coefficients C_3 and C_4. Although the inclination of 46.38° is in the resonance region, the coefficient C_5 is too small to dominate the periodic variation of the eccentricity. This shows that the dramatic effects of luni-solar secular resonances not only require the orbital inclination to be in the corresponding resonance region, but also require a large enough coefficient.

Fig. 14 and Fig. 15 show the orbital trajectory evolution with $i = 50°$and $i = 56.06°$ in the first 20 years, respectively. By comparing the two figures, we can clearly see how luni-solar secular resonances occur and observe marked differences. Changing the inclination will change the distribution of the time rate of eccentricity, i.e., the slope angle of the increase phase or decrease phase in Figs. 14 and 15. As stated in Eq. (22), the ratio of time rates of ω and Ω is also dependent on the inclination i of the considered orbit. Then, if the slope angle of the increase phase or decrease phase is consistent with the ratio of time rates of ω and Ω, the time rate of eccentricity will remain in the increase phase or decrease phase for a long time, as shown in Fig. 15, resulting in a very-long-period oscillation of the eccentricity in the long-term evolution. On the contrary, if the two angles are not close to each other, the orbital trajectory will pass through the increase phase or decrease phase much more frequently, as shown in Fig. 14, not generating a very-long-period oscillation of the eccentricity in the long-term evolution.

6. Conclusions

Based on the previous singly-averaged dynamical model that

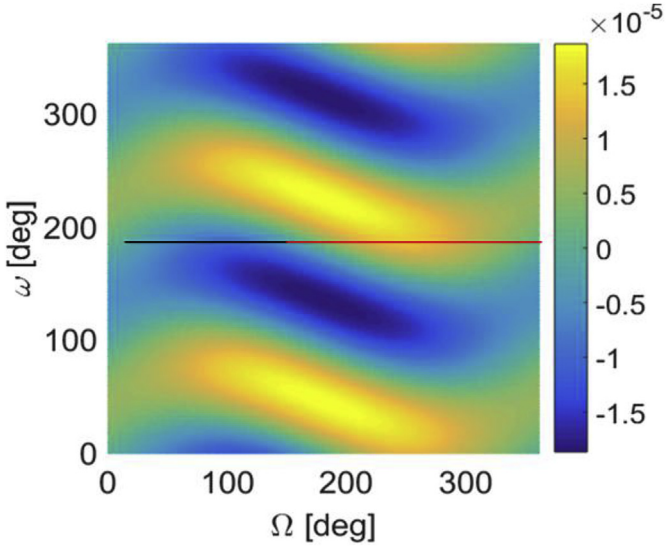

Fig. 6. Long-period eccentricity change per day with $i = 55^\circ$ calculated by Eq. (24) (the black and red line denote $\omega_0 = 178^\circ$). (For interpretation of the references to color in this figure legend, the reader is referred to the Web version of this article.)

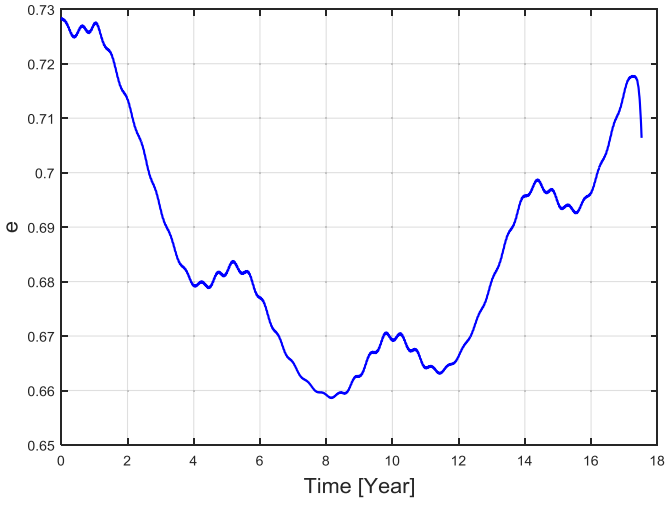

Fig. 7. Time history of the eccentricity e ($\Omega_0 = 70^\circ$).

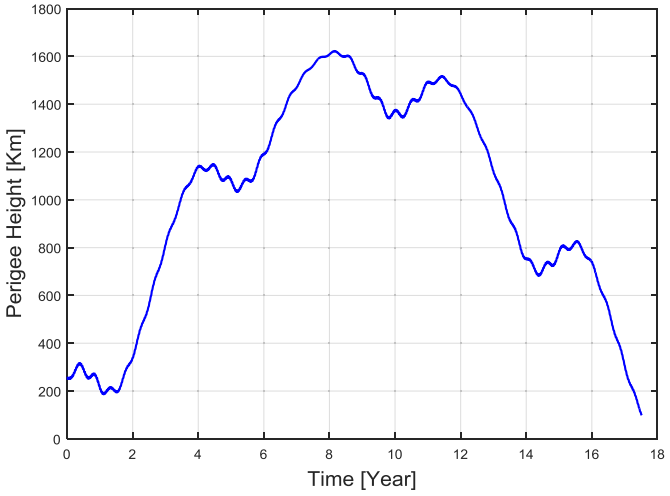

Fig. 8. Time history of the h_p ($\Omega_0 = 70^\circ$).

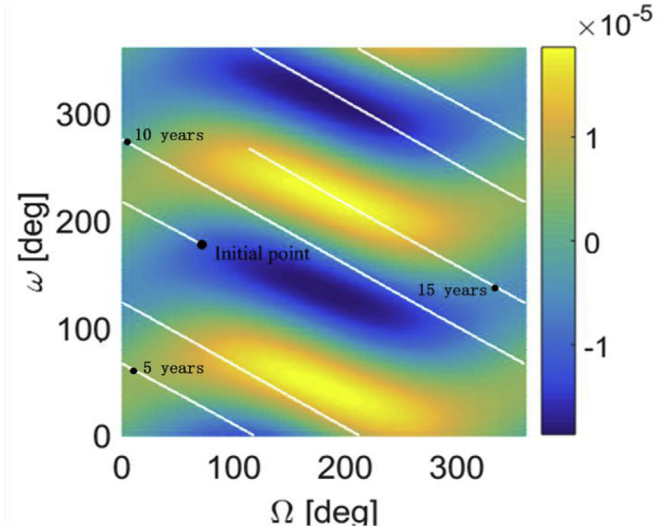

Fig. 9. Long-period eccentricity change per day with $i = 55^\circ$ calculated by Eq. (24) and the orbital trajectory evolution with $\Omega_0 = 70^\circ$.

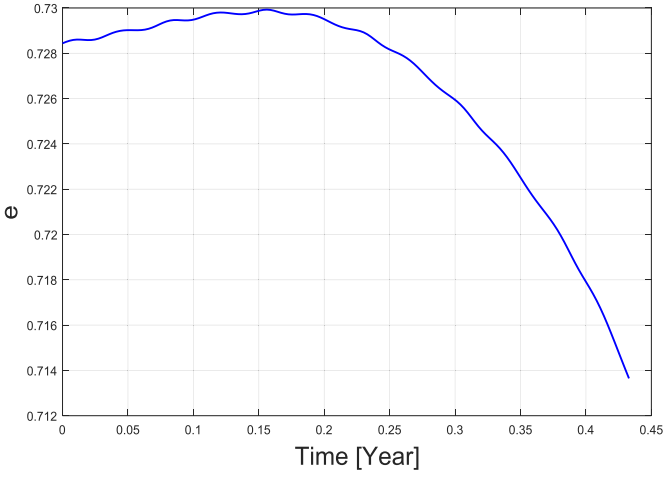

Fig. 10. Time history of the eccentricity e ($\Omega_0 = 250^\circ$).

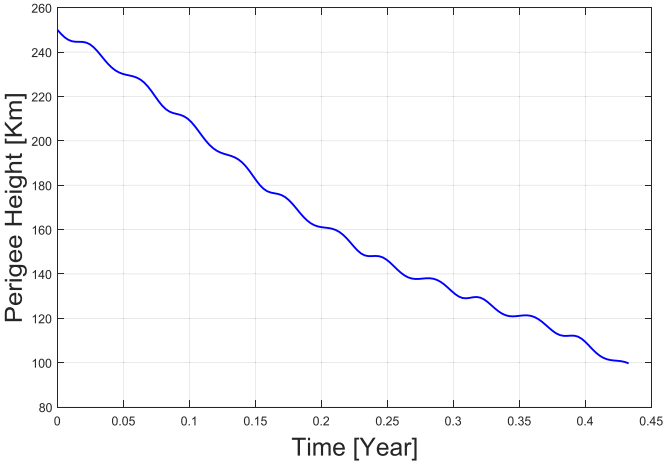

Fig. 11. Time history of the h_p ($\Omega_0 = 250^\circ$).

includes the Earth's oblateness, luni-solar perturbations, and atmospheric drag, this paper has established a more precise semi-analytical, singly-averaged orbital model for GTOs, by adding the effects of SRP. Numerical simulations compared with the STELA show that under the

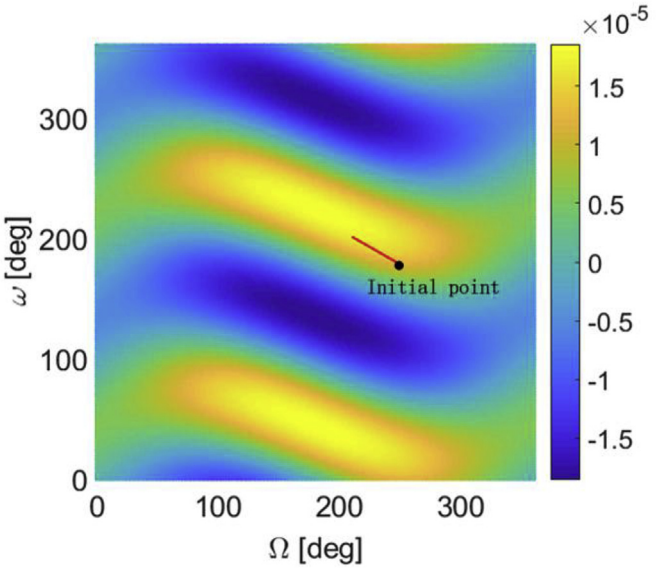

Fig. 12. Long-period eccentricity change per day with $i = 55^\circ$ calculated by Eq. (24) and the orbital trajectory evolution with $\Omega_0 = 250^\circ$.

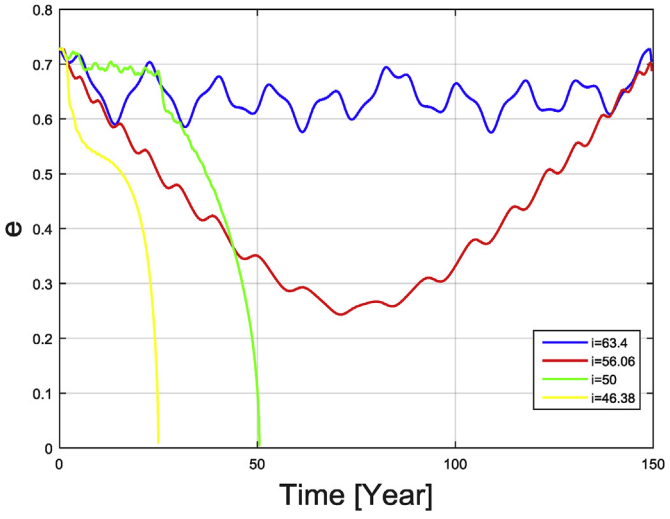

Fig. 13. Time histories of the eccentricity e with different inclinations.

effects of SRP, the orbit will show some different characteristics during the long-term evolution, and the semi-analytical orbital model given in the present paper can capture important features of the long-term evolution of GTOs better.

Then, we studied the long-term dynamical evolution and orbital resonances of the rocket upper stages in IGTOs using the established model and explained the underlying dynamical mechanism of the luni-solar secular resonances based on the doubly-averaged variational equation of ***e***. The results reveal us that the luni-solar secular resonances can be used to achieve the purpose of space debris mitigation. By adjusting the launch timing of the IGSO satellites of the Beidou satellite navigation system, i.e., the initial RAAN for the IGTO, the orbital lifetime can be very short under the effects of the luni-solar secular resonances.

Finally, by comparing and analysing long-term dynamical evolution of orbits with different initial inclinations, the mechanism and effects of luni-solar secular resonances are investigated in more details.

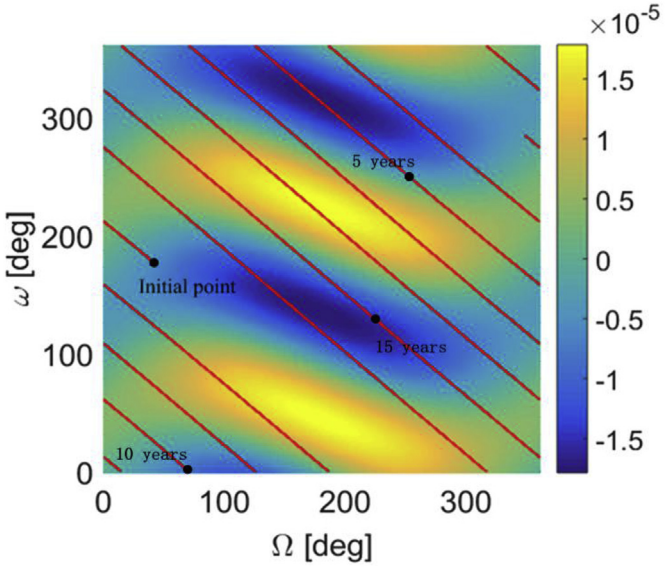

Fig. 14. Long-period eccentricity change per day with $i = 50^\circ$ calculated by Eq. (24) and the orbital trajectory evolution in the first 20 years.

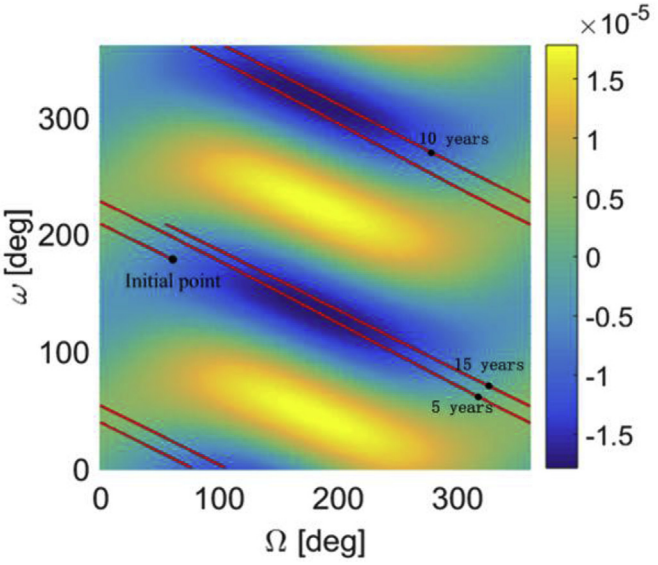

Fig. 15. Long-period eccentricity change per day with $i = 56.06^\circ$ calculated by Eq. (24) and the orbital trajectory evolution in the first 20 years.

Acknowledgments

The authors acknowledge the support of Fundamental Research Funds for the Central Universities.

References

[1] V. Morand, C.L. Fèvre, A. Lamy, et al., Dynamical Properties of Geostationary Transfer Orbits over Long Time Scales: Consequences for Mission Analysis and Lifetime Estimation, AIAA/AAS Astrodynamics Specialist Conference, 2013.
[2] A. Celletti, C. Efthymiopoulos, F. Gachet, C. Galeş, G. Pucacco, Dynamical models and the onset of chaos in space debris, Int. J. Non-Linear Mech. 90 (2017) 147–163.
[3] A. Rossi, C. Colombo, K. Tsiganis, et al., ReDSHIFT: a global approach to space debris mitigation, Aerospace 5 (2) (2018) 64.
[4] A.J. Rosengren, D.K. Skoulidou, K. Tsiganis, G. Voyatzis, Dynamical cartography of Earth satellite orbits, Adv. Space Res. 63 (1) (2019) 443–460, https://doi.org/10.1016/j.asr.2018.09.004.
[5] D. King-Hele, Lifetime prediction for satellites in low-inclination transfer orbits, J. Br. Interplanet. Soc. 35 (1982) 339–344.
[6] R.K. Sharma, P. Bandyopadhyay, V. Adimurthy, Consideration of lifetime limitation for spent stages in GTO, Adv. Space Res. 34 (No. 5) (2004) 1227–1232.

[7] V. Morand, C.L. Fèvre, A. Lamy, H. Fraysse, F. Deleflie, Dynamical properties of geostationary transfer orbits over long time scales: consequences for mission analysis and lifetime estimation, AIAA/AAS Astrodynamics Specialist Conference, no.AIAA2012–4C8,Minneapolis,Minnesota, 2012, 13–16 August.
[8] A. Lamy, C.L. Fèvre, B. Sarli, Analysis of geostationary transfer orbit long term evolution and lifetime, J. Aerosp. Eng. Sci. Appl. 4 (3) (2012) 12–27.
[9] Y. Wang, P. Gurfil, Dynamical modeling and lifetime analysis of geostationary transfer orbits, Acta Astronaut. 128 (2016) 262–276.
[10] Y. Wang, P. Gurfil, The role of solar apsidal resonance in the evolution of geostationary transfer orbits, Adv. Space Res. 59 (Issue 8) (2017) 2101–2116.
[11] D.K. Skoulidou, A.J. Rosengren, K. Tsiganis, et al., Dynamical lifetime survey of geostationary transfer orbits, Celest. Mech. Dyn. Astron. 130 (2018) 77.
[12] C.C. Chao, R.A. Gik, Long-term evolution of navigation satellite orbits: GPS/GLONASS/GALILEO, Adv. Space Res. 34 (2004) 1221–1226.
[13] A. Rossi, Resonant dynamics of Medium Earth Orbits: space debris issues, Celest. Mech. Dyn. Astron. 100 (2008) 267–286.
[14] L. Anselmo, C. Pardini, Orbital evolution of the first upper stages used for the new European and Chinese navigation satellite systems, Acta Astronaut. 68 (No. 11) (2011) 2066–2079.
[15] C. Pardini, L. Anselmo, Post-disposal orbital evolution of satellites and upper stages used by the GPS and GLONASS navigation constellations: the long-term impact on the Medium Earth Orbit environment, Acta Astronaut. 78 (No. 8) (2012) 109–117.
[16] F. Deleflie, A. Rossi, C. Portmann, G. Meris, F. Barlier, Semi-analytical investigations of the long term evolution of the eccentricity of Galileo and GPS-like orbits, Adv. Space Res. 47 (2011) 811–821.
[17] E.M. Alessi, A. Rossi, G.B. Valsecchi, L. Anselmo, C. Pardini, C. Colombo, H.G. Lewis, J. Daquin, F. Deleflie, M. Vasile, F. Zuiani, K. Merz, Effectiveness of GNSS disposal strategies, Acta Astronaut. 99 (2014) 292–302.
[18] T.V. Bordovitsyna, I.V. Tomilova, I.N. Chuvashov, The effect of secular resonances on the long-term orbital evolution of uncontrollable objects on satellite radio navigation systems in the MEO region, Sol. Syst. Res. 46 (No. 5) (2012) 329–340.
[19] T.V. Bordovitsyna, I.V. Tomilova, I.N. Chuvashov, Secular resonances as a source of dynamic chaoticity in the long-term orbital evolution of uncontrolled satellites, Sol. Syst. Res. 48 (No. 4) (2014) 259–268.
[20] E.D. Kuznetsov, E.A. Avvakumova, Dynamical evolution of space debris in the vicinity of GNSS regions, Acta Astronaut. 158 (2019) 140–147.
[21] M. Milankovitch, Kanon der Erdebestrahlung und seine Anwendung auf das Eiszeitenproblem, Canon of Insolation and the Ice-age Problem, Königlich Serbische Akademie (English translation by Israel Program for Scientific Trans-lations), Belgrade, 1941.
[22] A.J. Rosengren, D.J. Scheeres, Long-term dynamics of high area-to-mass ratio objects in high-Earth orbit, Adv. Space Res. 52 (8) (2013) 1545–1560.
[23] A. Lemaitre, N. Delsate, S. Valk, A web of secondary resonances for large A/m geostationary debris, Celest. Mech. Dyn. Astron. 104 (2009) 383–402.
[24] S. Hughes, Earth satellite orbits with resonant lunisolar perturbations. I. Resonances dependent only on inclination, Proc. R. Soc. Lond. A 372 (1980) 243–264.
[25] C.C. Chao, An Analytical Integration of the Averaged Equations of Variation Due to Sun–Moon Perturbations and its Application, Technical Report, SD-TR-80-12 The Aerospace Corporation, El Segundo, CA, October, 1979.
[26] A. Celletti, C. Gales, Dynamics of resonances and equilibria of low Earth objects, SIAM J. Appl. Dyn. Syst. 17 (2018) 203–235.
[27] E.M. Alessi, G. Schettino, A. Rossi, Natural highways for end-of-life solutions in the LEO region, Celest. Mech. Dyn. Astron. 130 (34) (2018).